

The role of porosity on degradation of concrete under severe internal and external brine attack in confined conditions

Sherzer, G. Lifshitz; Ye, G.; Schlangen, E.; Kovler, K.

DOI

[10.1016/j.conbuildmat.2022.127721](https://doi.org/10.1016/j.conbuildmat.2022.127721)

Publication date

2022

Document Version

Final published version

Published in

Construction and Building Materials

Citation (APA)

Sherzer, G. L., Ye, G., Schlangen, E., & Kovler, K. (2022). The role of porosity on degradation of concrete under severe internal and external brine attack in confined conditions. *Construction and Building Materials*, 341, Article 127721. <https://doi.org/10.1016/j.conbuildmat.2022.127721>

Important note

To cite this publication, please use the final published version (if applicable). Please check the document version above.

Copyright

Other than for strictly personal use, it is not permitted to download, forward or distribute the text or part of it, without the consent of the author(s) and/or copyright holder(s), unless the work is under an open content license such as Creative Commons.

Takedown policy

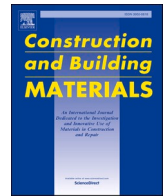
Please contact us and provide details if you believe this document breaches copyrights. We will remove access to the work immediately and investigate your claim.

Green Open Access added to TU Delft Institutional Repository

'You share, we take care!' - Taverne project

<https://www.openaccess.nl/en/you-share-we-take-care>

Otherwise as indicated in the copyright section: the publisher is the copyright holder of this work and the author uses the Dutch legislation to make this work public.



The role of porosity on degradation of concrete under severe internal and external brine attack in confined conditions

G. Lifshitz Sherzer^{a,*}, G. Ye^b, E. Schlangen^b, K. Kovler^c

^a Department of Civil & Mineral Engineering, University of Toronto, 35 Saint George Street, Toronto, Canada

^b Microlab/Section of Materials and Environment, Faculty of Civil Engineering and Geosciences, Delft University of Technology, 2628 CN Delft, The Netherlands

^c Faculty of Civil and Environmental Engineering, Technion - Israel Institute of Technology, Haifa, Israel

ARTICLE INFO

Keywords:

Brine attack
Multiscale analysis
Strength
Service life
Durability
Confinement

ABSTRACT

It has been observed that a trench wall embedded in the soil of the Dead Sea has lost strength and is deteriorating due to brine attack. This phenomenon demonstrates that concrete wall structural stability and durability can be seriously endangered. Yet conventional analysis using macroscopic models is considered an oversimplification, as it neglects the existing micro-cracking and other nonlinearities that are endemic to such deterioration. The current study describes a multiscale formulation for estimating the anticipated reduction in strength of a concrete wall exposed to both external and internal briny water. Our methodology provides an upscale formulation to predict concrete response under aggressive environmental and partially confined conditions. The proposed method uses the concept of a “fictitious” water-to-cement (w/c) ratio to express the microstructural changes that cause an increase in material porosity, thus reflecting the material’s degradation through leaching. Simulation results indicate that under the partially confined conditions representing actual ground pressure, the trench wall will remain stable for a service life of 40 years. Furthermore, the proposed model was experimentally calibrated and validated and found in agreement with experimental results.

1. Introduction

1.1. Description of trench wall and its environmental conditions

The Dead Sea is located at the lowest point on Earth and is probably the best example of a hypersaline (340–380 g/l of salinity) lake [1]. The composition of its briny water differs from that of other saline lakes because of its high concentrations of dissociated calcium, magnesium, and chloride ions. An 18-km long trench wall with a thickness and depth of 0.8 and 33 m, respectively, was recently constructed for the rehabilitation of a dike, encapsulating a 75 km²-large evaporation basin belonging to the Dead Sea Works Ltd. (DSW), and located in the southern part of the Dead Sea. As a result of erosion and associated loss of sealing, seepage water losses have increased in the trench wall over the years. Additionally, the associated formation of cavities in the core area led to settlement and cracks in the dike and eventually formation of sinkholes. This dike was recently strengthened to prevent its possible collapse owing to the difference between the upstream and downstream levels of the Dead Sea water and to reduce seepage losses [2].

The excavated trench was supported by a slurry consisting of local silt and clay mixed with brine from the Dead Sea. A mixture consisting of blast furnace cement CEM III 42.5/A (containing slag and considered highly resistant to aggressive environmental attack), wadi gravel (gravel sand with fines), and brine was used to produce “brine concrete” on-site. Before the lamellae were concreted, a thin steel sheet pile profile was installed in the trench to ensure a sealing effect of the lamellae’s cut-off during any future heightening activity and to resist heavy earthquakes, either of which could lead to considerable bending moments in the cut-off. As the constructed wall is embedded in the ground, it is exposed to ground pressure and self-weight. The requirement of the designer of the wall is that its strength not deteriorate to the values than could not resist its self-weight.

In marine constructions, it has been proven that steel corrosion takes place in the long run, mainly where the water table and ground meet the fresh air. In this work, the wall is constructed (embedded) permanently in the compacted ground of the dike; thus, corrosion of the steel sheet pile is not considered to be of (much) concern. A view of the cross-section’s wall (containing two materials: the brine concrete and the

* Corresponding author.

E-mail addresses: gili.lifshitzsherzer@utoronto.ca (G.L. Sherzer), G.Ye@tudelft.nl (G. Ye), Erik.Schlangen@tudelft.nl (E. Schlangen), cvrkost@technion.ac.il (K. Kovler).

<https://doi.org/10.1016/j.conbuildmat.2022.127721>

Received 14 February 2022; Received in revised form 27 April 2022; Accepted 1 May 2022

Available online 18 May 2022

0950-0618/© 2022 Elsevier Ltd. All rights reserved.

steel), together with its lateral cut-off cross-section, is shown in Fig. 1. See also [2].

Concerns persist regarding the durability of this type of concrete against both external and internal attacks of the extremely aggressive brine of the Dead Sea. It is known that the brine of the Dead Sea, which contains magnesium chloride ($MgCl_2$), chemically reacts with concrete-forming brucite ($Mg(OH)_2$), which consequently converts the calcium silicate hydrate (C-S-H) of the cement gel into magnesium-silicate-hydrates (M-S-H). These new reaction products are weak and therefore may cause deterioration and loss in the strength of the cementitious compounds by breaking down the binder matrix bonding aggregates. Such deterioration poses dangers to the dike safety, owing to the rise in sea level; likewise, increasing desertification (owing to climate change) leads to the growth of salt content. In other words, the Dead Sea has a high evaporation rate that causes a decrease in the lake's water level, thereby increasing the density and salt content of its brine [3]. A more detailed description of the concrete damage resulting from this phenomenon can be found in [4–6].

The concrete of the trench wall embedded in the ground under aggressive conditions of the Dead Sea can lose its strength and quickly deteriorate. Therefore, the durability and structural stability of the walls can be seriously endangered. Conventional analysis using macroscopic models is considered an oversimplification because of micro-cracking and other nonlinearities. The methodology proposed in this study uses the concept of a “Fictitious” water-to-cement (w/c) ratio, which is related to microstructural changes occurring owing to brine attack on concrete. The wall material is exposed to extremely aggressive attacks from (1) the brine used as mixing water during concrete preparation on site, since using brine instead of tap water in concrete compositions is unprecedented in engineering practices worldwide, and (2) the external brine of the Dead Sea, since the ground of the dike is rather permeable.

The rationale behind using concrete prepared with brine and its simultaneous exposure to the external brine attack to strengthen the dike stems from the assumption that the resulting mechanical response of the wall material to the expected deterioration mechanisms may be significantly diminished owing to the confinement from the surrounding compacted ground.

It must be emphasized that the “Fictitious” w/c ratio introduced by the authors is not a mathematical ratio of the mass of water to that of cement in the concrete mix; rather, it is a conceptual ratio indicating mainly the increasing material porosity over time, which results in a loss of strength.

The “Fictitious” w/c ratio is a correlation factor representing the degradation of the mechanical performance of concrete subjected to aggressive conditions. This ratio can likewise be applied to chemical

simulations resulting in microstructure change that consequently represents the leaching phenomenon of cementitious materials. Leaching occurs wherever concrete comes into contact with water having a pH value less than that measured in the pore solution of cementitious materials; other chemical reactions can also cause this phenomenon. Leaching leads to the transfer of ions from external water to the concrete pore solution, causing dissolved ions such as calcium to leach out; these ions are then transported in solution to another location outside the concrete wall. This process increases porosity, permeability, and diffusivity of concrete, thereby degrading its mechanical performance.

The leaching effect has been modeled using various types of empirical methods [7,8]. In addition, a 2D numerical study of the mineralogy of leached cement resulted in cracked materials [9], while another work used a continual 3D numerical model within thermodynamic specification and phase stability exposed to low pH solutions [10]. Herein, we used a different concept, “Inverse Analysis,” to represent the leaching effect by controlling the w/c ratio based on experiment results of compressive strength at variable leaching times. Controlling the deterioration of the material through w/c ratio makes sense it plays a key factor when the leaching effect occurs.

The method developed here uses three levels of concrete upscaling, as described below.

1.2. Cement scale

Focusing on fine resolution, the cement paste scale (hereafter, “cement scale”) is defined as a heterogeneous material composed of solid products derived from the hydration process that are between 1 and 50 μm in size. The HYMOSTRUC3D model developed by Van Breugel et al. [11–14], addressing the level of hydration of cement products resulting in microstructure change related to their expansion, was applied. Accordingly, the cement particles were modeled as spheres that grew throughout the hydration process. Designed as a 3D explicit model, HYMOSTRUC3D requires data related to cement components, such as the w/c ratio, amount of cement, mineralogical composition, cement fineness as measured by the Blaine apparatus, temperature of the mix of Portland and blended cements, and specimen geometry. In our approach, the “Fictitious” w/c ratio representing the destructive effect of brine was used. The Rosin–Rammler sieve curve, as presented in [15], was chosen to describe the cement particle size distribution.

The lattice model [16,17], which can effectively predict material behavior, crack pattern, and microcrack propagation based on the microstructure, mortar, and concrete structure, was applied to characterize the damage process. This model discretizes the continuum of materials, as characterized by Timoshenko beam elements [18]. The

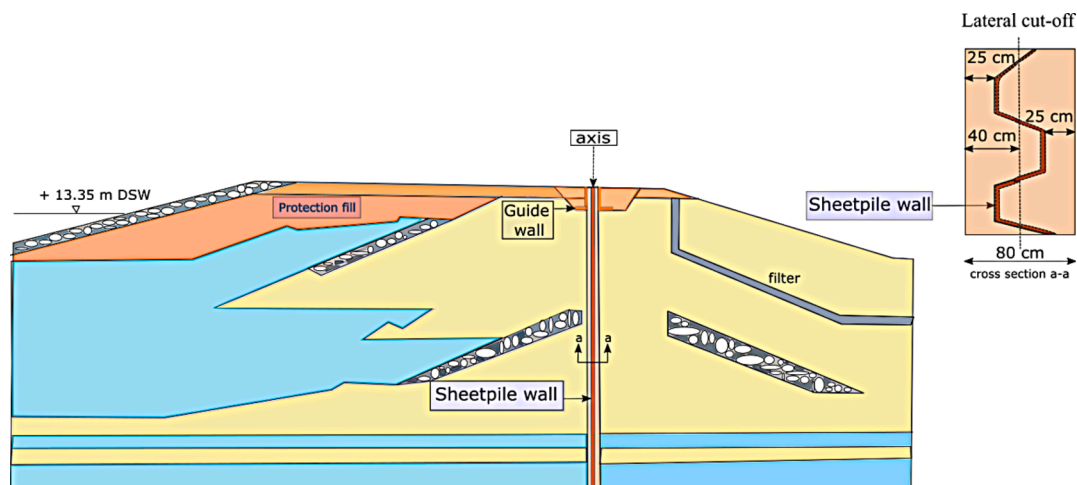


Fig. 1. Cross-section of the wall (including the lateral cut-off) embedded in the ground.

lattice network was constructed based on the structure of a unit cell. First, the resolution/voxel is controlled by dividing the unit cell into voxel cells. Then, one random node is parked in every sub-cell located in each voxel cell. Next, the neighboring nodes are connected by beam elements. The randomness of these nodes controls the degree of disorder in the material, and as the element orientation influences the cracks, it affects the fracture behavior. While the choice of randomness must include a sufficient amount of heterogeneity, a slight difference must be maintained between the lengths of the elements. After generating the mesh, the mechanical properties were assigned to each component depending on its location in the microstructure. Finally, depending on the type of test being simulated, the boundary conditions were assigned to the unit-cell surfaces. Lattice damage analysis determines the critical element (e.g., the highest stress-to-strength ratio at each incremental step). At every stage of the analysis, the critical element is eliminated from the structure until the entire structure fails. This elimination approach is related to the brittle fracture law [19], in which the maximum stress is calculated as.

$$\sigma = \alpha_N \frac{F}{A} + \alpha_M \frac{(M_{xOy}, M_{xOz})}{W} \quad (1)$$

where A is the area of the cross-section, W is the section modulus, α_N and α_M are the “normal force influence factor and the bending influence factor”.

1.3. Mortar-s scale

The second scale (hereafter, “mortar-s”) represents a mortar made with fine sand. The materials included in this scale were cement paste (matrix) and sand particles (inclusions). The mechanical properties for the matrix scale were scaled up from the cement paste analyses, wherein the size of the sand particles was in the range of 0.13–0.8 mm. The geometrical structure of the mortar-s scale was evaluated using the Anm model developed by Qian et al. [20], which is unique in its ability to create unit cells of particles that are characterized irregularly as well as the interface layer and matrix (cement). These particles are inserted into the unit cells from the largest to the smallest, while overlapping among them is prevented. The Anm model can be implemented using either periodic or non-periodic boundary conditions. In this study we chose to implement periodic boundary conditions that mirror the particles of the unit-cell surface on their opposite surfaces. The data necessary for execution of Anm model include specimen size, particle size (as measured by width) distribution, as well as aggregate mass and density. The outcome of this model represents the mortar structure, which served as an input for the lattice model [16,17] subsequently applied to analyze the damage process on the mortar scale.

1.4. Concrete scale

The larger scale dealt with in this study is the concrete (more accurately, mortar made with coarse sand) scale, labeled “mortar-a4.” Its mechanical matrix properties were scaled up from those in the mortar-s analysis, and the size distribution of the aggregates was set to 0.8–4 mm. Additionally, for this scale, Anm [20] and lattice models [16,17] were used.

It should be noted that all scales have an interface layer that surrounds the inclusions. In addition, in this study, concrete-confined compression properties were attained directly using the up-scaled properties of the cement-scale response under compression. These confined compression properties represent the failure mechanism of pore collapse, and the methodology to simulate this failure mechanism is described in [21].

The methodology proposed in the current study was applied to evaluate the durability and stability of the concrete wall in a dike owned by the Dead Sea Works, made of concrete containing brine as the mixing

water. As the brine from the salt layers located beneath the wall foundation attacks the cement matrix, the continuing degradation of the core material, which itself contains the brine, is a major concern. Therefore, the primary research goal was to assess the durability and service life of the wall, originally designed to last for 40 years. In this study, the strength reduction was examined via unconfined uniaxial compression of concrete cylinders performed at four different ages, and the final test was conducted at the age of 120 d following the construction of the wall. Because these tests were conducted under unconfined conditions, the contribution of confinement was not considered. Thus, the evaluation of the confined concrete strength is required for a realistic prediction of the wall stability. Furthermore, it is known that chemical reactions can be aggressive under unconfined conditions because of the alkali-silica reaction (ASR), which results in the formation of microcracks in the cementitious matrix [22]. The mechanical effect of confined concrete results in the initial yielding owing to pore collapse, which is followed by a hardening behavior caused by pore closure [23]. This mechanical effect leads to an increase in compressive strength with the level of confinement. The compressive strength can also be evaluated by evolutionary artificial neural networks [24]. In a previous study [21], it was observed that the unit cell of cement for the lattice model represents concrete behavior under compaction and pore collapse; therefore, the same cement paste scale was chosen for testing.

2. Methodology

In this section, we describe our up-scaling method for predicting the compressive strength of concrete at 40 years of service life under aggressive environmental conditions and confinement pressure. Here, the primary challenge in prediction stems from the concrete composition, which incorporates brine instead of tap water, and external brine conditions. Our approach for modeling this unique type of concrete is divided into the following sub-steps.

In the first step, we developed an approach to define a “Fictitious” w/c ratio that increases over time as a factor for the HYMOSTRUC3D material model developed by Van Breugel et al. [11–14]; this approach considers the effect of brine on concrete strength. This effect was then incorporated multiple times into this material model to evaluate various microstructures as a function of exposure time to brine. In the second step, we used these microstructures as an input for the lattice mechanical model developed by Qian et al. [16,17] to simulate the material behavior under different types of loads.

The three pathways are shown in Fig. 3. The first pathway shows our method of up-scaling, specifically from the cement scale to the concrete scale, which we subsequently validated with an unconfined compression test of the samples drilled from the actual concrete wall. The second pathway shows simulated compressive tests with completely confined conditions to examine the effect of confinement, while the third pathway shows simulated compressive tests performed under partially confined conditions representing the ground pressure.

In the first pathway starts with the material model simulation. The novelty of this approach is the development of a method to correlate strength reduction to the material porosity, using a “Fictitious” w/c ratio that increases over time, which in turn increases the porosity and changes the microstructure. For this pathway, our objective was to up-scale from the cement paste to the concrete scale with two material models, namely HYMOSTRUC3D (cement scale) and Anm (mortar and concrete scales). These two models were then combined with the lattice mechanical model, which requires input parameters obtained from the stress-strain curve under tension. Thus, the up-scaling from the cement scale to the concrete scale achieved by a parameter-passing scheme was evaluated using a tensile simulation. In addition, the microstructure was added to the lattice model, and a lattice simulation was performed to evaluate the mechanical properties to be used as input for the larger mortar-s scale. Additional information regarding the model applicable conditions is presented in a schematic diagram (Fig. 2).

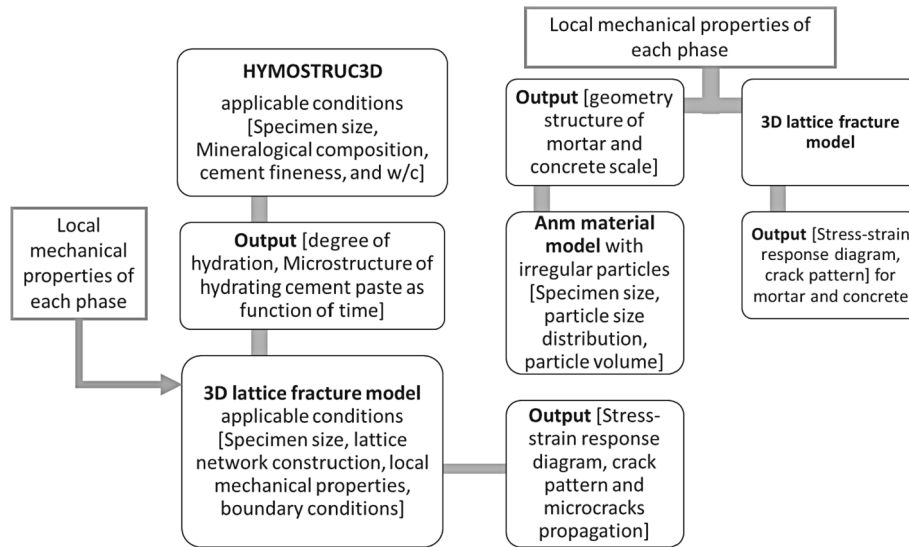


Fig. 2. Framework for the combined models and applicable conditions.

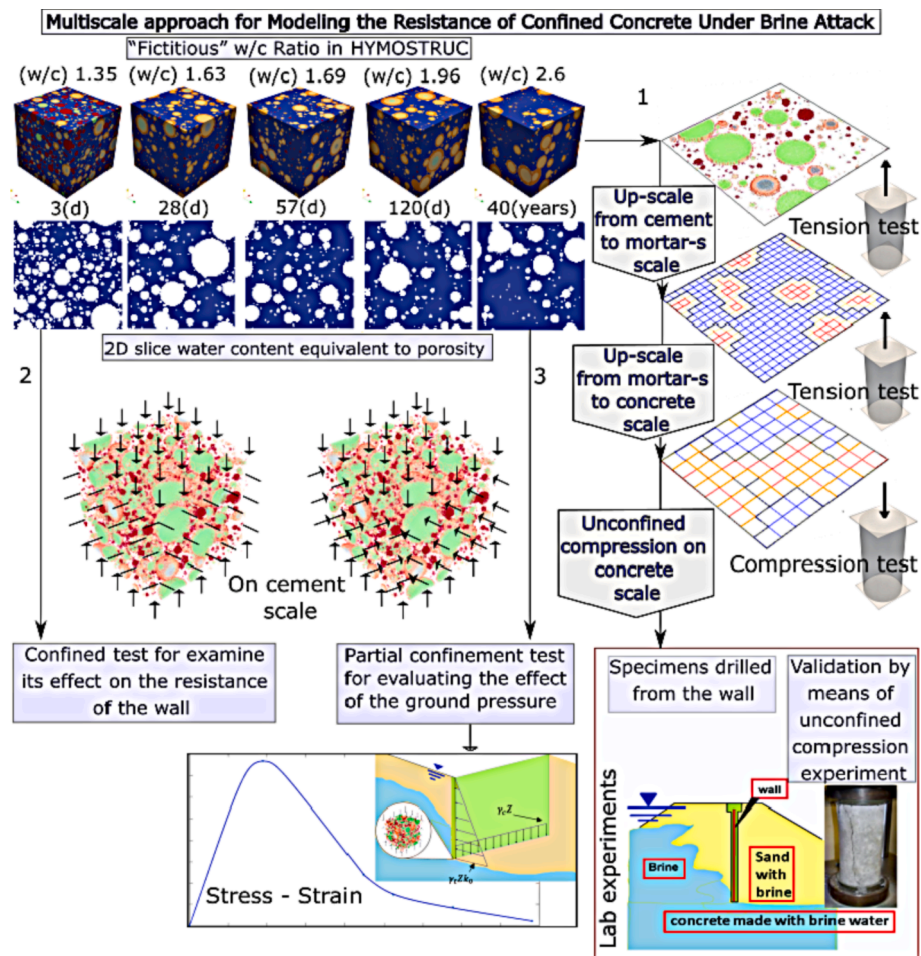


Fig. 3. Workflow for modeling the resistance of concrete made with brine in confined conditions.

To simulate the mortar-s scale, the Anm model, which creates the unit cell of this scale, was first used. It was then combined with the lattice model to perform tensile simulations for up-scaling to the concrete scale. After up-scaling, any boundary condition can be selected. To validate the fitting of the experiments, we used unconfined compression

tests performed on a concrete scale. For this scale, the Anm model was also used to obtain the unit cell of the concrete combined with the lattice model under unconfined conditions. This was performed to predict the stress-strain curves. The validation was achieved by comparing the stress-strain curve obtained from the simulation with that from the

experiments performed on the wall samples.

The second and third pathway selections were initiated using the proposed microstructure approach. Next, the damage mechanism of the cement paste scale was obtained from lattice model simulations. The objective of the second pathway was to simulate the compressive tests under completely confined conditions so that we could examine the confinement effect, the purpose of which was to simulate partially confined uniaxial compression loads representing the actual ground loads. In both these pathways, the cement scale represents the unit cell of the concrete properties under confined conditions.

3. Materials

The proposed methodology was applied to a case study of a given wall located in the Dead Sea; therefore, all the material properties were used as input parameters for the numerical simulations based on this case study.

3.1. Brine specifications

The composition of the Dead Sea brine is as follows: K^+ : 7965 ppm, Mg^{2+} : 47,704 ppm, Ca^{2+} : 18540.5 ppm, Na^+ : 18,246 ppm, Cl^- : 213408.5 ppm, SO_4^{2-} : 250.5 ppm, HCO_3^- : 260.5 ppm; and specific gravity: 1.253 g/cm³.

For the sake of comparison, the composition of seawater brine is presented as follows: K^+ : 395.3 ppm, Mg^{2+} : 1278 ppm, Ca^{2+} : 409.9 ppm, Na^+ : 10,679 ppm, Cl^- : 19,162 ppm, SO_4^{2-} : 2680 ppm, and HCO_3^- : 24.84 ppm.

3.2. Concrete material specifications

The concrete design of the wall [2] located in the Dead Sea is detailed according to the data required for the simulations related to each scale, ranging from the cement scale to concrete scale. The mix design contained a blast furnace cement CEM III 42.5/A produced by Nesher Israel Cement Enterprises, Ltd. Its specifications are as follows:

1. Mineralogical composition of clinker and gypsum in the cement (35%): C_3S , 55%; C_2S , 20%; C_3A , 6%; C_4AF , 15%
2. Clinker and gypsum fineness in the cement (Rosin–Rammler distribution):

$$F(x) = 1 - e^{-bx^n} \quad n = 1.05771, \quad b = 0.04282.$$

3. Chemical composition of the slag (65%): Al_2O_3 —10.9%, SiO_2 —36.17%, MgO —7.39%, CaO —42.75%, Fe_2O_3 —0.72%, SO_3 —2%, Na_2O —0.46%, K_2O —0.29%
4. Slag fineness (Rosin–Rammler distribution): $F(x) = 1 - e^{-bx^n}$ ($n = 1.4457$, $b = 0.0112$)
5. Chemical composition of the cement paste: CaO —51.85%, SiO_2 —27.59%, Al_2O_3 —6.87%, TiO_2 —0.57%, Fe_2O_3 —2.48%, Mn_2O_3 —0.26%, MgO —4.34%, SO_3 —3.54%, Na_2O —0.91%, P_2O_5 —0.74%, SrO —0.56%, K_2O —0.29%, Cr_2O_3 —0.02%
6. Minimum particle diameter: 1 μm
7. Maximum particle diameter: 50 μm
8. The initial chloride content 30‰ Cl/m out of cement paste
9. At a curing temperature of 20 °C, the average temperature of groundwater in the Dead Sea area was 24 °C (see [25]), while the temperature in the trench wall was lower than the ambient temperature or that in the upper layer of the Dead Sea water; therefore, it was set to 20 °C.

The mix design of the wall is also given in Table 1.

We evaluated the “Fictitious” w/c ratio for each concrete age to ensure the validity of our model for concrete in brine. For this, we used a

Table 1
Mix composition.

Parameter	Value
Cement content C [kg/m ³]	350
Brine water to cement ratio w/c [-]	1.37
Salt concentration [%]	31.5
Water-to-Salts [%]	2.17
Aggregate and sand content [kg/m ³]	2216
Maximum aggregate size D_a [mm]	16

tool that allows a connection between the chemical effects owing to the brine attack and the loss of concrete strength by introducing an increasing “Fictitious” w/c , which represents the gradually degrading material microstructure; that is, the porosity mimics the material degradation. Therefore, the “Fictitious” w/c ratio (represented by the content of porosity in our simulation) for each concrete age was evaluated according to its experimental compressive strength. To evaluate the “Fictitious” w/c ratio for each concrete age, we adopted Eq. (2), which provides the “Fictitious” w/c ratio according to the concrete compressive strength by the well-known Abrams’ law, used by concrete technologists [26]. This report was based on the local guidelines for concrete mix design and is still considered to be the most accepted method for representing the strength of concrete as a function of the w/c ratio.

$$\sigma = \frac{A}{B^{w/c}} \quad (2)$$

where A and B are constants, and w/c is the “Fictitious” water to cement ratio. These constants were obtained by curve fitting between the curve obtained from [26], which is valid for CEM 42.5, and Eq. (2). For example, for the presented simulation and cement type CEM 42.5, the coefficients were determined as $A = 125.4$ and $B = 9.29$.

The appropriate “Fictitious” w/c ratios required for each simulation were evaluated based on the experiments of unconfined compressive strength performed on a variable duration of exposure to brine, as presented in Table 2. The compressive strength for the variable duration of exposure to brine obtained from the experimental results was used in Eq. (2) to determine the “Fictitious” w/c ratio (see Table 2). The other information shown in Table 2 includes the experimental scatter of the compressive strength obtained from the four cylindrical specimens, microstructure corresponding to each data point, and 2D slice of water content of the unit cell.

Additionally, we attempted to establish a relationship between the chemical effects and loss of mechanical strength of the interface layers between the sand and aggregate particles. The subsequent reduction of strength is detailed in Section 5.2 and summarized in Table 5.

In addition, samples drilled from the wall at variable depth locations at the same time were used to measure and weight the “Dry” density of the specimen. The experiment result of the “Dry” density as a function of depth is shown in Fig. 4.

The results presented in Fig. 4 show the dry density measurements of the samples taken from different wall locations. The absence of a correlation between the density and wall depth and low scatter of results indicates that the porosity of hardened concrete and its initial strength are independent of the depth.

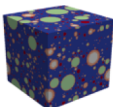

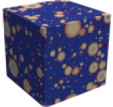

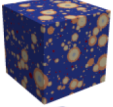

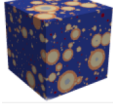

The mechanical properties of fine sand and other aggregates are assumed, according to [17], as follows: Young’s modulus $E = 70,000$ MPa, shear modulus $G = 29,000$ MPa, tensile strength $f_t = 24$ MPa, and uniaxial unconfined compressive strength $f_c = 240$ MPa.

The sieve analysis results of the aggregates are presented in Table 3.

4. Macroscopic experiment

First, the mixture was tested to examine concrete workability by a flow diameter test following EN 12350-5. The diameter of concrete flow

Table 2
Compressive strength, time, “Fictitious” w/c, of the unit cell, and 2D slice of water content of the unit cell.

Mean strength σ (MPa)	Coefficient of variation (%)	Experimental exposure duration (d)	Time (h)	Time-dependent fictitious w/c	Unit-cell form fictitious w/c	2D slice of water content of the unit-cell
6.21	15	3	72	1.35		
3.28	30	28	672	1.63		
2.92	24	57	1368	1.69		
1.6	18	120	2880	1.96		

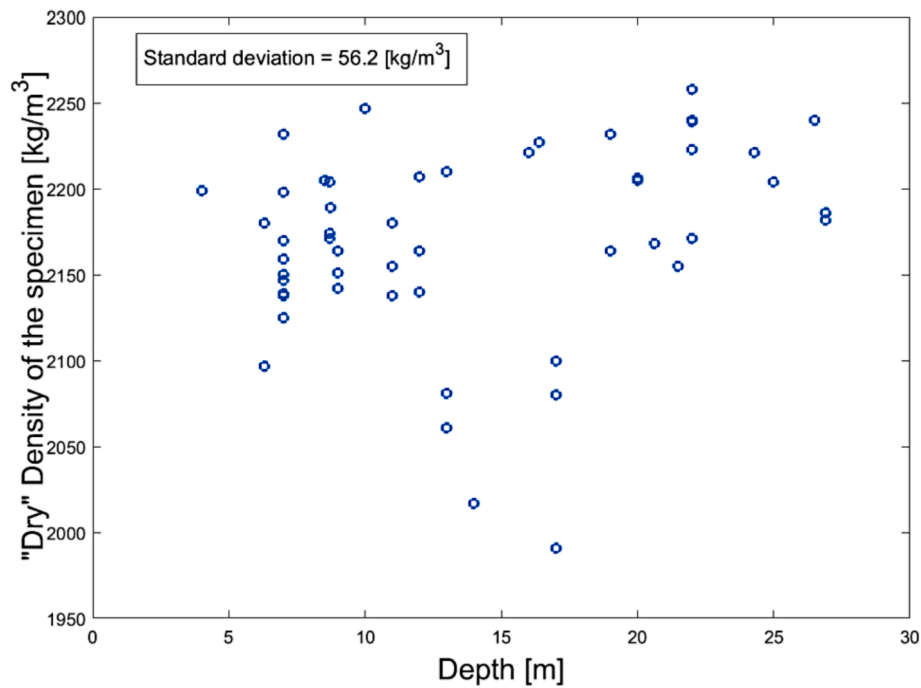


Fig. 4. “Dry” density measurements of concrete cores taken from different depths of the wall.

Table 3
Sieve analysis results of the aggregates.

Type of sands	Sieve range (mm)	Mass percentage (%)
Fine sand particles	0.13–0.8	100
Aggregate particles	0.8–1.5	14
Aggregate particles	1.5–2.5	29
Aggregate particles	2.5–3.0	29
Aggregate particles	3.0–3.5	14
Aggregate particles	3.5–4.0	14

was found to be in the range of 540–620 mm. Later, unconfined compressive tests were carried out on specimens drilled from the wall located in the Dead Sea (see [2] for more details). These specimens, drilled from the wall approximately half a year after it was cast, were

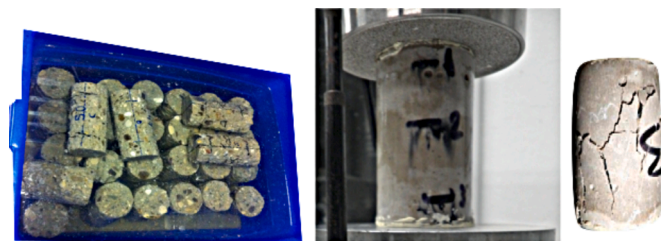


Fig. 5. Concrete specimens placed in brine water (left), unconfined compressive tests (middle), and concrete after testing (right).

then placed in brine water. Testing was conducted at different durations of immersion, see Fig. 5.

The specimens drilled from the concrete wall had standard cylindrical shapes with diameters and heights of 37 and 60 mm, respectively. Following immersion in brine for different periods of time, the specimens were tested at (3, 28, 57, and 120 d) to estimate the loss of strength owing to the brine attack. The results of each experiment were subsequently used to calibrate and validate the numerical models. The mineralogical component of the clinker and gypsum and the chemical component of the slag were determined by X-ray diffraction (XRD) and inductively coupled plasma (ICP) analyses, respectively. The amounts of clinker, gypsum, and slag, particle size distribution, minimum and maximum particle sizes, and curing temperatures are presented in Section 3.2. The slag in this type of cement is the main hydraulic component, and its reaction rate is slower than that of normal Portland cement. This slow reaction leads to the formation of further CSH phases and results in a lower heat of hydration than in regular Portland cement.

The sieve analysis of the sand is summarized in Table 3. Uniaxial unconfined compression tests were conducted with high friction (HF) boundary conditions, which characterize the degree of friction resulting from direct contact between the specimen and steel loading plates without lubrication. The dependence of the unconfined uniaxial compressive strength versus the duration of exposure to brine is presented in Table 2, while the experimental damaged cement zone is depicted in Fig. 9. The strength results were used to calibrate and validate the numerical models and estimate the concrete strength at the end of a service life of 40 years. However, should one wish to predict the realistic risk of failure for the service life of a wall, the effects of partial confinement must be considered. Confinement is expected to slow down concrete expansion, chemical reactions, and loss of strength.

5. Microstructure modeling of cement paste

5.1. Input parameters

The validated HYMOSTRUC3 model [14] was used to simulate the cement hydration process and ultimately create the cement paste microstructure. Simulations were performed for the material mix design, which is described in detail in Section 3. The microstructure was assigned a variable “Fictitious” w/c ratio corresponding to the duration of exposure to the brine for the specimens tested for unconfined compression. The “Fictitious” w/c values of 1.35, 1.63, 1.69, and 1.96, according to the exposure duration, are listed in Table 2.

To demonstrate that the wall was well-designed a design life of 40 years, another simulation was performed using the HYMOSTRUC3D model [14]. This 40-year simulation was accomplished by using the microstructure at the age of 317 d, at which point the cement products reached approximately 99% of their hydration. These simulations were performed for the previously mentioned material mix design. The “Fictitious” w/c ratio corresponding to a 40-year exposure duration was evaluated using Equation (3), which is logarithmic and based on the four experimental datasets presented in Table 2, as shown in Fig. 6.

$$\frac{w}{c} = 0.1507 \cdot \ln(\text{time}(d)) + 1.1571 \quad (3)$$

The “Fictitious” w/c ratio, thus determined for a 40-year period, was 2.6. Fig. 6 shows the curve fitting between the experiments and Eq. (2).

To account for the material degradation caused by the brine attack, each exposure duration was simulated with the HYMOSTRUC3D model discontinuity in such a manner that the w/c parameter could be changed rather than set as a fixed value, thus allowing the formation of different microstructures with increasing water content. In this argument, we assume that the simulations from time 0 to the evaluated time, with its appropriate w/c , can be used to evaluate the concrete strength. This

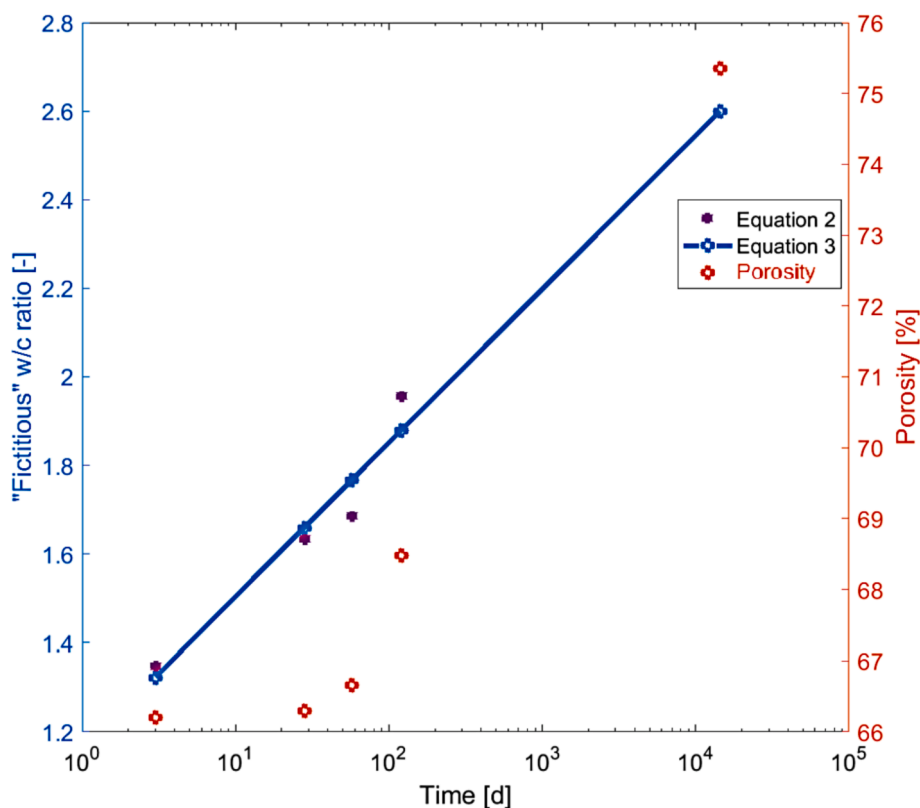


Fig. 6. The y-axis represents the “Fictitious” w/c ratio (left) and the percentage of porosity volume out of the cement unit cell (right), while the x-axis represents duration of exposure to the brine with a log scale view. Also presented is a 2D slice of water content (blue) of the cement unit cell at each data point.

assumption does not represent the actual material degradation process; however, it provides an appropriate response. We adopted this as a calibration process that provided logical outputs in the order of magnitude.

5.2. Simulation results

The predicted microstructures at ages 3, 28, 57, and 120 d were labelled according to the duration of exposure of the specimen to brine. Simulations were performed at 3, 28, 120, and 40 years to ensure consistency in the ages of the macroscopic experiments and their corresponding simulations. The resulting microstructural changes in the concrete versus the duration of exposure to brine for the 100-mm cubes are presented in Fig. 7.

6. Unconfined simulation tests Up-scaled from cement to concrete

This section describes a comparison between the results of an experimental uniaxial unconfined compression test, as detailed in the material section and the up-scaled strategy [27], from the cement paste scale to the concrete scale. This concrete scale is the scale of the experimental validation results presented in Section 5. In addition, a calibration at 28 d was performed to obtain the mechanical interface properties, a validation at 57 d, and an analysis of the cut-off unconfined wall at the end of 40 years is presented here.

6.1. Estimation of cement paste mechanical properties

To reduce the computational time, the simulation was performed by a two-steps approach (see [27]).

Initial homogenization step. The specimen size allocated for the cement paste was dismantled to 1000 sub-specimens, of size $10 \times 10 \times 10 \mu\text{m}^3$, at ages of 28, 57, and 317 d, and 40 years, as presented in Section 4.2. The lattice simulations of all sub-specimens one after the other were carried out in an automated manner. The verification and validation with experiments on the proposed lattice model are presented in [19]. For the cement paste scale the uniaxial tension simulation was

chosen to scale up the required mechanical properties of the cement paste scale; representative points of the resulting stress–strain curve were used for the properties of the matrix of the mortar scale. In addition, High-friction (HF) boundary conditions were similarly assigned for the tensile simulation. Hard contact, known as HF, was obtained by preventing displacements and rotations on the loading faces and allowing free motion on the remainder surfaces. The elastic properties of the variable phases were investigated as published in [28], and the tensile strength was evaluated from its hardness, and the compressive strength was assigned through an approximate estimation by multiplying the tensile strength by 10, as suggested in [17]. The mechanical properties of the solids on the cement scale are listed in Table 4. The interface mechanical properties, displayed in Eqs. (4) and (5), were calculated according to the formulae published in [17].

$$\frac{2}{E_I} = \frac{1}{E_A} + \frac{1}{E_B} \quad (4)$$

$$f_H = \min(f_{IA}, f_{IB}) \quad (5)$$

where E_A and E_B are the moduli of solids A and B , respectively, and E_I is the interface layer module.

A resolution of $1 \mu\text{m}/\text{voxel}$ was chosen for each voxel cell in this study, and the randomness was set to 0.5, as recommended in [17]. After generating the mesh, the mechanical properties must be assigned based on its location in the microstructure of each element. The local phases include unhydrated cement, slag, inner products, outer products, and CH. The elements connecting two different phases were assigned the interface properties, while the pores were not assigned an element as they did not contribute to the global performance. Thus, the number of material types created for this simulation was 15, as presented in

Table 4
Specifications of lattice model inputs used for the cement paste scale.

No.	Element type	Young's modulus E (GPa)	Shear modulus G (GPa)	Tensile strength f_t (GPa)	Compressive strength f_c (GPa)
1	Unhydrated Cement	135.0	52.0	1.80	−18
2	Interface — Unhydrated Cement and Slag	100.5	41.8	1.60	−16
3	Interface — Unhydrated Cement and Inner	49.0	20.0	0.24	−2.4
4	Interface — Unhydrated Cement and Outer	38.0	15.2	0.15	−1.5
5	Interface — Unhydrated Cement and CH	53.0	22.0	0.26	−2.6
6	Slag	80.0	33.0	1.60	−16
7	Interface — Slag and Inner	43.6	18.1	0.24	−2.4
8	Interface — Slag and Outer	34.5	14.3	0.15	−1.5
9	Interface — Slag and CH	46.7	19.5	0.26	−2.6
10	Inner product	30.0	12.0	0.24	−2.4
11	Interface — Inner and Outer	25.0	10.0	0.15	−1.5
12	Interface — Inner and CH	31.5	12.6	0.24	−2.4
13	Outer product	22.0	8.9	0.15	−1.5
14	Interface — Outer and CH	26.4	10.6	0.15	−1.5
15	CH	33.0	13.2	0.26	−2.6

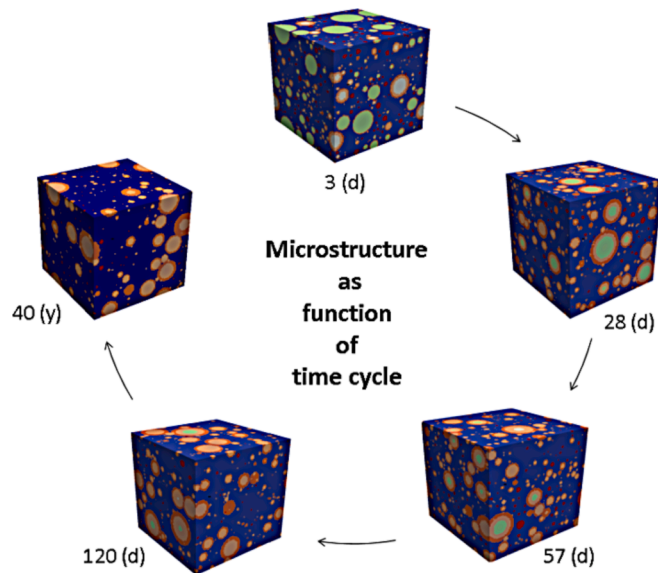


Fig. 7. Microstructure simulation for the input “Fictitious” w/c ratio defined for each respective exposure duration: $w/c = 1.35$ at 3 d; $w/c = 1.63$ at 28 d; $w/c = 1.69$ at 7 d; $w/c = 1.96$ at 120 d; and $w/c = 2.60$ at 40 years (the porous cement paste is represented by dark blue, un-hydrated cement by gray, and slag by bright green; the inner hydration product is shown in bright orange, outer hydration product in dark orange, and CH-calcium hydroxides in red).

Table 5

Interface material properties between the cement matrix and sand particles for the mortar-s scale and aggregate particles, and mortar-s matrix for the concrete scale.

No.	Element Type	Young Modulus E (MPa)	Shear Modulus G (MPa)	Tensile Strength f_t (MPa)	Compression Strength f_c (MPa)
2	Interface — Fine Sand and Cement 28 d	41,681	17,033	3.805	-38.05
2	Interface — Fine Sand and Cement 57 d	36,080	14,744	3.23	-32.3
2	Interface — Fine Sand and Cement 120 d	26,565	10,887	2.425	-24.25
2	Interface — Fine Sand and Cement 40 years	1775	143	0.16	-1.6
2	Interface — Aggregates and Mortar-s t 28 d	43,017	17,579	3.93	-39.3
2	Interface — Aggregates and Mortar-s 57 d	36,597	14,956	3.343	-33.43
2	Interface — Aggregates and Mortar-s 120 d	27,419	11,237	2.505	-25.05
2	Interface — Aggregates and Mortar-s 40 years	1832	143	0.16	-1.6

Table 4.

Following homogenization step. The original specimen size allocated for the cement paste was employed in the simulations using the lattice model with a resolution of 10 $\mu\text{m}/\text{voxel}$. The elements were of the same size as the resolution and were assigned to the mechanical properties of the output resulted from the stress–strain curve for each sub-specimen from the initial homogenization step. Tensile simulations were conducted for the ages of 28, 57, and 317 d and 40 years, which provided the stress–strain curve of the cement paste for evaluating the mechanical properties of the matrix of the mortar-s scale (see Fig. 8).

6.2. Scaling up from the cement to mortar-s scale

The mortar scale was composed of a cement paste that functioned as a matrix, sand particles, and an interface layer bonding the particles and the matrix together. The mechanical properties of this sand are obtainable in Section 3.2, while the interfaces between the sand and cement paste for different ages are listed in Table 5. Multilinear curves were generated from the simulations described in Section 5.1 (see Fig. 8), and the mechanical properties were defined accordingly. The lattice model applied for the tensile simulations was assigned the same boundary condition as described in Section 5.1. To ensure cost-effective simulation while maintaining a good quality of results, we selected a specimen size of $2 \times 2 \times 2 \text{ mm}^3$ or 2.5 times the maximum particle size from the unit-cell of the mortar-s scale. This ratio was sufficient to consider the material homogeneity, as recommended in [29]. This up-scaling method required the higher scale to be of a similar or finer resolution than that of the lower scale; therefore, the resolution chosen was 0.1 mm/voxel, or

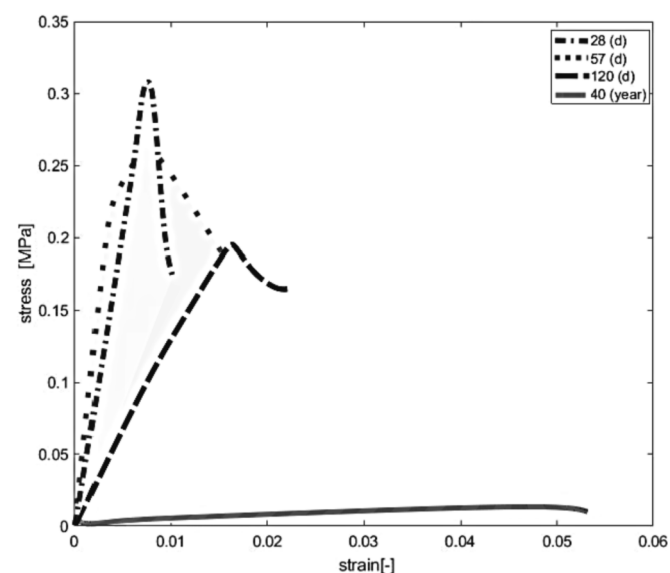


Fig. 8. Tensile simulation of the cement paste at 28, 57, and 120 d, and 40 years. The tensile strength at 57 d was lower than at 28 d by 14.92%; tensile strength at 120 d was lower than at 28 d by 36.26%; and tensile strength at 40 years was lower than at 28 d by 95.74%.

one that was equal to the specimen size of the cement scale. (Additional information can be found in [17]: The geometrical structure of the mortar scale was generated using the Anm material model simulation [20]. For this purpose, the Anm model input parameters included the unit cell size of the mortars, sieve analysis of the sand, as presented in Table 3, a mass of 0.004044 g, and a density of 0.00265 g/mm^3 , which is related to sand particles.

Mechanical properties of the cement paste (Fig. 8), sand particles (see [17]), and interface bonding the sand are fed to the lattice model. These interface parameters were calibrated to the experimental results of the unconfined compression strength at 28 d, as presented in Table 5. In addition, the mechanical properties of the sand–cement paste interface (see Table 5) were reduced for the ages of 57 d and 40 y based on the referenced interface properties at 28 d by the same percentage difference as the cement strength result (Fig. 8). Furthermore, the simulation on this scale resulted in a crack pattern and the stress–strain curve of the mortars, as displayed in Figs. 9 and 10, respectively.

As expected, the more extended the duration of exposure to brine, the more extensive the damaged zone, as shown in Fig. 9.

6.3. Scaling up from mortar-s to concrete scale

The concrete scale represents mortar-a4, containing the matrix (mortar-s), aggregates smaller than 4 mm, and an interface layer bonding the aggregates and the matrix. A small concrete cube ($10 \times 10 \times 10 \text{ mm}^3$) was chosen to ensure practical simulation time and accuracy of the outcomes. In addition, this piece was cut from the middle zone of the original cylindrical specimens with diameters and heights of 37 and 60 mm, respectively, (see Fig. 10). The selected resolution was 1 mm/voxel [17], and the Anm model was applied to evaluate the geometrical structure of the concrete scale [20]. The Anm model input parameters included the unit cell size of this scale, as mentioned above, the sieve analysis properties of the aggregate (presented in Table 3), a mass of 1.1795 g, and a density of 2,650 kg/m^3 related to the aggregate particles.

6.4. Estimation of unconfined compressive strength of concrete at 40 years

Simulations were performed on the mortar-a4 scale to calibrate mechanical interface layer properties at 28 d, validate compressive strength at 57 d, and analyze unconfined compressive wall strength after 40 years. It should be noted that these calibrations were corrected for the size effect caused by performing this simulation on smaller specimens cut out from the original cylindrical specimens. The impact of maximum aggregate size was also correlated to the cut-of size, with the maximum aggregate limited to 4 mm instead of 32 mm as used in the field.

For the mortar scale simulation, the mechanical properties of the matrix were estimated from the stress–strain curve (Fig. 10) as an input. The aggregate mechanical properties are presented in Section 3, and the mechanical interface properties are listed in Table 5. The simulation type, damage zone of the concrete scale, and experimental damage zone are presented in Fig. 11.

The calibration was accomplished by changing the interface

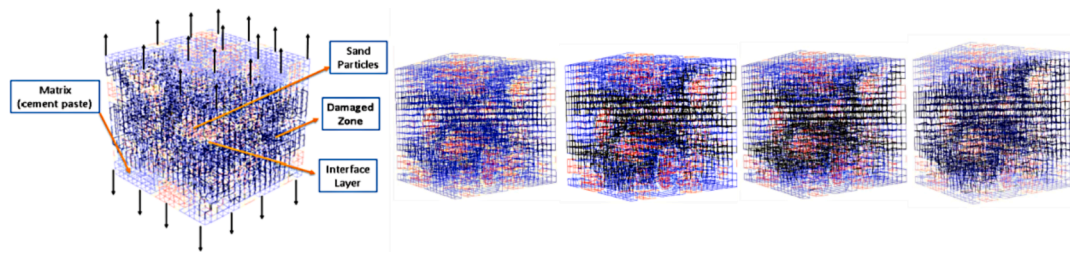


Fig. 9. Uniaxial tension analysis of the mortar-s scale (cement paste in blue; sand particles in red; interface layer in yellow; and damaged elements in black), and damage patterns from 28 d to 40 years (from left to right).

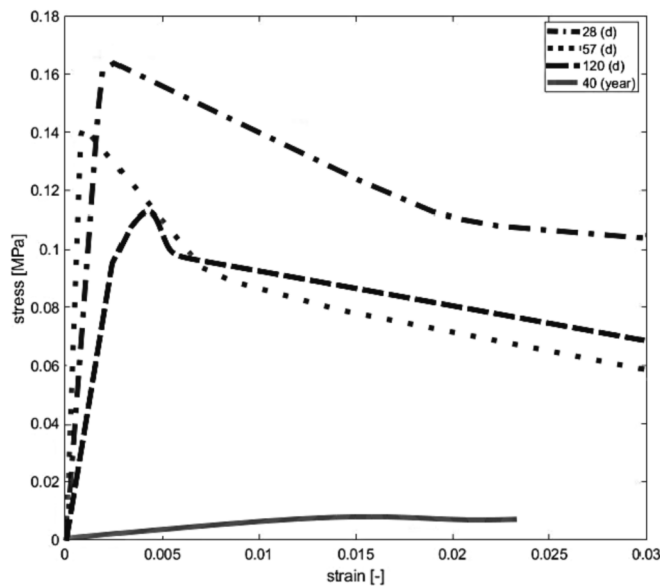


Fig. 10. Mortar-s stress-strain curve.

mechanical properties and performing a numerical simulation until a good fit was obtained between the mortar-a4 numerical results and experimental results at 28 d. The validation was achieved by comparing the numerical results with the experimental results at 57 and 120 d using the reduced aggregate-cement paste interface results, as explained in Section 5.2. The strength at 40 years was predicted using the reduced interface results, as explained in Section 5.2 (see Fig. 8). The stress-strain curves for these simulations are shown in Fig. 12.

Fig. 12 presents the calibration and validation results. The approximation errors between the numerical simulations and the experimental results were 3.25% and 8.68% for 57 and 120 d, respectively; thus, the validation process demonstrated a remarkably good fit between the results. This well fit supports a reliable analysis of the unconfined compression stress value. In addition, as can be seen in Fig. 12, the simulation of the wall at 40 years is predicted to fail due to its 33-m self-weight (0.5 MPa). However, it must be noted that this prediction was unrealistic because of the effect of the ground pressure on the behavior of concrete. In conclusion, the compression simulation with partial confinement needs to be analyzed for the stability of the wall after 40 years, thus indicating the need for a partial confinement compressive simulation test (Section 7).

The unconfined compressive simulations were compared with the experiments described above (see Section 4 and Eq. (2) concerning the material porosity using the “Fictitious” w/c ratio obtained from Eq. (3)). We then expressed the compressive stress as a function of time to represent the degradation of the material resulting from the microstructural changes, which in turn were caused by increasing the material porosity via the “Fictitious” w/c ratio (shown in Fig. 13).

Fig. 13 reveals a good correlation between the simulation and Eq. (2)

with the “Fictitious” w/c ratio obtained from Eq. (3) and the experiments performed at early ages. The main contribution of this research is the expression of microstructural changes that cause an increase in material porosity via the “Fictitious” w/c ratio. This approach is strongly based on fundamental physical and mechanical principles, while Eq. (2) is well accepted within the engineering community.

7. Confined simulation tests

A three-dimensional lattice damage model [17] was used to evaluate the pore collapse properties of the cement paste at different exposure durations (3, 28, 57, and 120 d) with equivalent water-to-cement ratios of 1.35, 1.63, 1.69, and 1.96, respectively (Table 2). These specific exposure durations of the cement paste were chosen so that the simulations would be consistent with the duration of exposure of the concrete specimens used to brine on the macroscopic scale during the uniaxial unconfined compression experiments. The microstructures obtained from Section 4.2, were used as inputs for the lattice model.

Simulations were performed on the cement paste scale according to age and material porosity via the “Fictitious” w/c ratios, as mentioned above, to evaluate the strength under full confinement. A uniaxial strain test was also performed, in which the specimen was loaded under compression in the longitudinal direction, while transverse expansion was prevented. Allocating a longitudinal displacement, these uniaxial strain simulations were performed, and the transverse expansion was prevented by inhibiting all deformations and rotations on these surfaces (see Fig. 14). On the faces that were loaded with an incremental displacement, the nodes were constrained against rotation and displacement perpendicular to the load direction. In addition, all nodes were free to fail under tension or compression. The cement paste unit cell size used was $100 \times 100 \times 100 \mu\text{m}^3$, while the lattice network chosen for this simulation was quadrangular. Furthermore, the chosen resolution was $1 \mu\text{m}/\text{voxel}$, with a random parameter of 0.5. The mechanical properties of the cement paste used in the lattice simulation are listed in Table 4.

The generated load-displacement diagram was subsequently converted into a stress-strain diagram, as shown in Fig. 14, for the four different simulations described above.

The initial peak point beyond which the slope changes, as shown in Fig. 14, represents the initial yield compressive stress σ_{c0} . The simulation on the cement paste scale was chosen to represent the failure criterion of pore collapse because only this scale includes the porosity of the lattice model. The unit cell of the cement scale was equivalent to the concrete scale; therefore, the unit cell of the concrete scale could be replaced with that of the cement scale because the failure of the concrete under confined conditions would involve a physical collapse of the porous material microstructure at its initial peak point. Under these conditions, we expected an initial peak value caused by the breakage of the pore walls and collapse of the pores, followed by hardening owing to the closure of the pores. The failure criterion of the pore collapse was represented in the cement scale, while the compressive strength under unconfined conditions was represented on the mortar-a4 scale, which fitted the unconfined compression experiment test to represent the

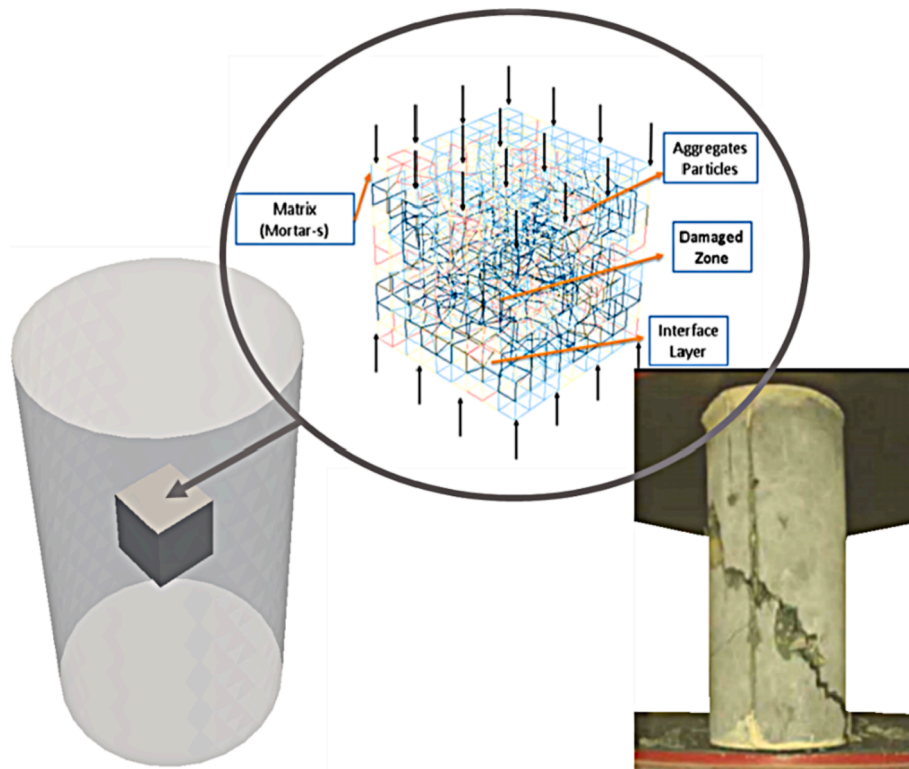


Fig. 11. Simulation of uniaxial compression test on mortar-a4 scale (mortar-s in blue; aggregate particles in red; interface layer in yellow; and damaged elements in black), taken from its cut-off from the middle zone of the original cylindrical specimens (left), and experimental crack pattern at 28 d (right).

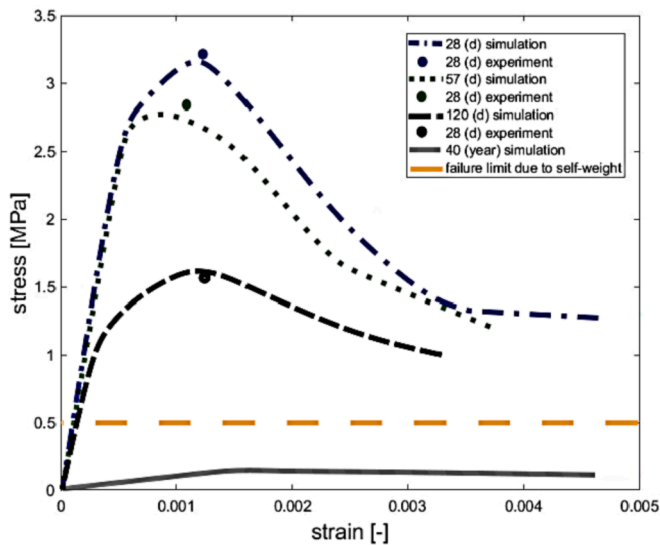


Fig. 12. Experimental results of uniaxial compression test and numerical validation using mortar-a4 scale calibration (blue line: numerical simulation at 28 d; dark blue circle: compressive experimental strength at 28 d; green line: numerical simulation at 57 d; bright green circle: compressive experimental strength at 57 d; purple line: numerical simulation at 120 d; bright purple circle: compressive experimental strength at 120 d; red line: numerical simulation at 40 years; and dashed orange line: failure limit owing to the gravitation forces of the 33-m deep wall).

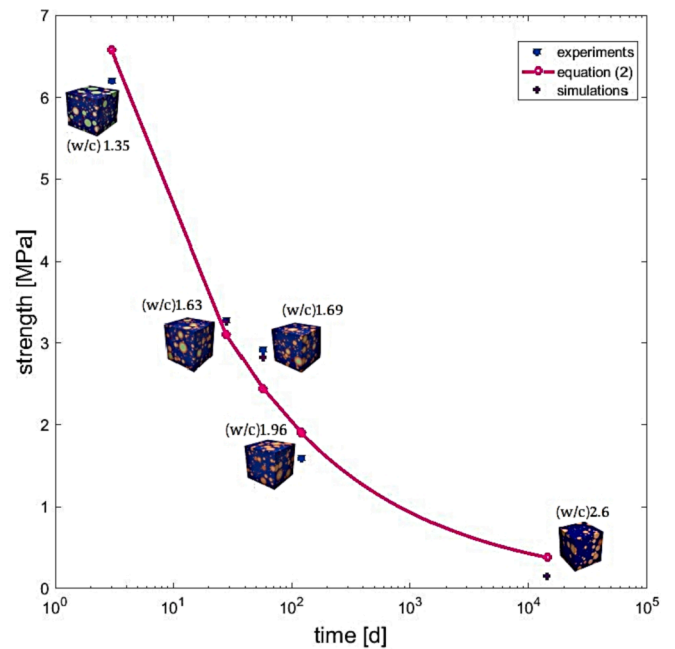


Fig. 13. Predicted compressive strength–time dependence of unconfined concrete exposed to brine at each unit-cell data point.

failure criterion of other parameters.

8. Partial confinement (ground pressure) – compressive simulation tests

Next, simulations were performed on the cement paste scale under partial confinement resulting from the ground pressure to establish that

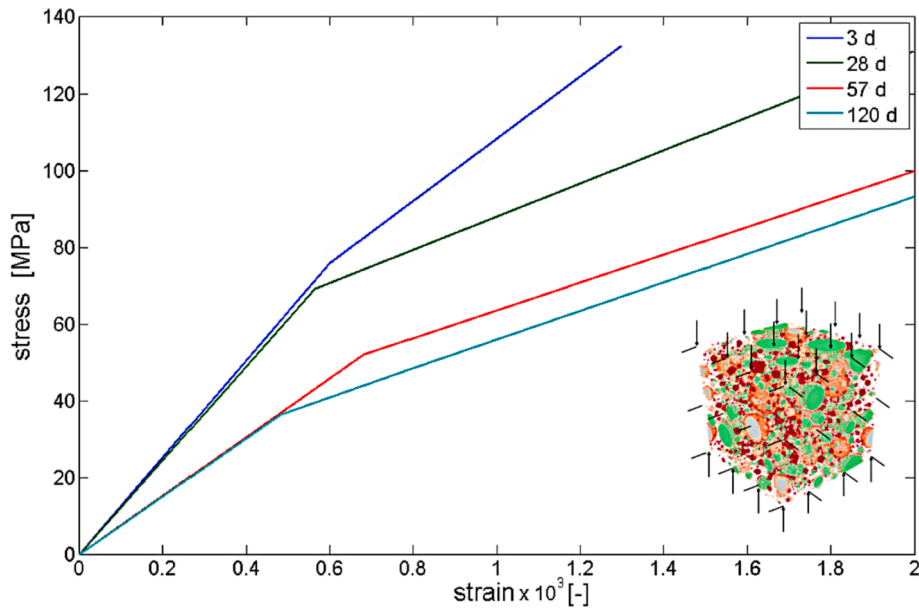


Fig. 14. Uniaxial fully confined strain tests on the cement paste scale for four different ages.

the wall was well-designed, as originally intended, for a service life of more than 40 years. The microstructure obtained from the HYMOSTRUC3D model analyzed for 40 years was used as the input for the subsequent triaxial lattice simulation. The unit cell was applied with the boundary conditions, which corresponded to the loads actually applied on it (self-weight – vertical and ground pressure – lateral). The unit cell was loaded with displacements instead of loads, while the same ratio was maintained, assuming a linear relationship. The lateral displacement boundary conditions were imposed in the opposite direction to that of the unit-cell expansion owing to the compression load and partly prevented its expansion owing to ground pressure. In other words, this simulation was performed by applying displacements to all the surfaces of the specimen, with a constant ratio of 1.27 between the vertical and lateral displacements. This ratio corresponded to the maximum amount of vertical pressure owing to the self-weight of the 33-m wall (concrete density \times height of the wall), to the lateral ground pressure under 33 m (ground density \times height \times ground coefficient), as shown in Fig. 15. On these faces loaded with an incremental displacement, the nodes were constrained against rotations and displacement, and all the nodes were free to fail under tension or compression. The unit cell size of the cement paste was $100 \times 100 \times 100 \mu\text{m}^3$, the resolution was chosen to be $1 \mu\text{m}/\text{voxel}$, and the randomness was set to 0.5. Furthermore, the lattice network chosen for this simulation was quadrangular. The stress–strain curves obtained from the triaxial tests are shown in Fig. 15.

The yield compressive stress obtained from the partial confinement compressive simulation was 3.8 MPa (see Fig. 15), whereas the

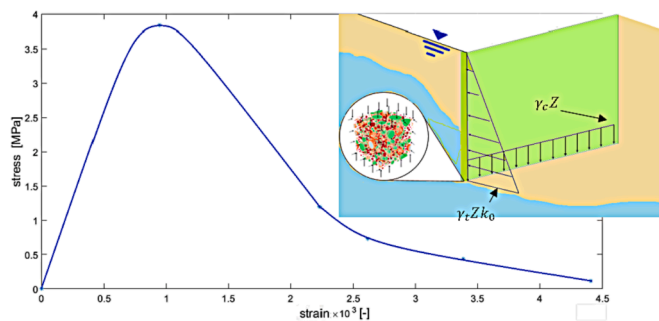


Fig. 15. Stress–strain curve of the compressive simulation test under partial confinement.

maximum pressure loaded onto the specimen as a function of the self-weight of the 33-m wall was 0.5 MPa. Therefore, it can be concluded that the longevity and durability intended for the wall's life service of 40 years were well-planned.

9. Validation study for concrete with leaching effect

This section focuses on the validity of our approach in achieving accurate porosity volume out of a cement specimen subjected to leaching by comparing it to experimental results from the work of F. H. Heukamp [30]. This experiment was designed to measure the porosity volume, identified by the mass change between a saturated and oven-dried asymptotically leached specimen of cement paste. Note that the time to reach asymptotic leaching was calculated in the work [30] and found to be 60 (d). The cement paste type used was Type I Portland cement, and its mineralogical composition was 35%: C3S, 50–70%; C2S, 15–30%; C3A, 5–10%; and C4AF, 5–15%. The estimated compressive strength of the leached cement paste was 3.2 MPa.

The work of [30] provided all of the data needed to estimate porosity volume using the methodology proposed in the current work. First, Sec. 3.2 using Abrams' law [26] for correlating compressive strength with the w/c ratio was repeated, but this time constants A and B of Eq. (2) were obtained by curve fitting to the Type I Portland cement, (the diagram appears in [26]). Coefficients were determined as $A = 146.5$ and $B = 9.29219$; at this point, the "Fictitious" w/c ratio defined for the leached cement paste with a compressive strength of 3.2 MPa was 1.715. Next, a simulation of the microstructure was performed for the leached cement paste. While the input used for this simulation contained the defined w/c and the specified mineralogical composition, the simulation outcome also provided data related to porosity volume. In addition, the results included experimental scatter and model uncertainties (see Fig. 16).

The median observed between the experiment and simulation was found to be 8.73%, with the largest error 16.56% and the smallest error 0.48%. Indeed, this fit is very good, indicating that our method provides a sophisticated and straightforward solution for including the leaching effect in the model.

10. Summary and conclusions

This study proposed a multiscale approach for evaluating the

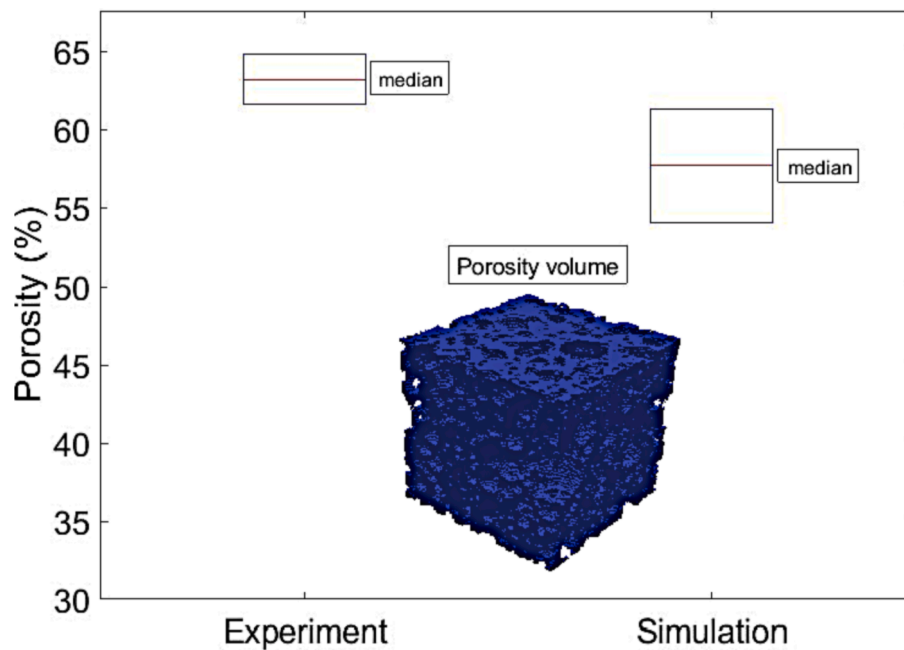


Fig. 16. Porosity volume as estimated experimentally and from simulation on the cement level, including method uncertainties.

strength of concrete under different confinement conditions and extremely aggressive brine attack from (1) brine used as mixing water during concrete manufacturing on site, and (2) the external brine of the Dead Sea penetrating through the compacted but rather permeable ground of the dike. Brine attacks lead to swelling, increased permeability, loss of strength, expansion, and cracking.

The main contribution of this multiscale approach is its ability to appropriately represent brine attacks through material porosity via the “Fictitious” w/c ratio.

The first step of the process comprised calibration and validation using unconfined simulation tests performed according to the experimental results. Consequently, it was demonstrated that the models used in this study, together with the upscaling method, can predict the behavior of concrete based on a mix design. In addition, cracking from the brine attack increased as the duration of exposure to this condition was prolonged, as shown in this study on the cement paste scale. In addition, uncertainties such as the scatter of the experimental results are presented.

The current case study analyses showed that at 40 years of brine attack, the wall owing to its self-weight would fail under unconfined conditions. The wall is embedded in the ground. Thus, confined conditions indeed exist on-site, leading to unrealistically low predicted strength for the simulation of unconfined conditions, as shown in (Fig. 12).

The process followed in this study comprised fully confined compressive simulations performed to demonstrate the phenomenon of confinement. These simulations were performed on a cement paste scale, which is the only scale that contains the porosity properties. Under fully confined conditions, we expected an initial peak value caused by the breakage of the pore walls and collapse of the pores, followed by hardening owing to the closure of the pores. Therefore, the failure criterion of the pore collapse was represented in the cement scale (i.e., equivalent to the concrete scale), while the compressive strength under unconfined conditions was represented on the concrete (mortar-a4) scale.

The third step involved simulations of compression under partial confinement owing to the ground pressure at 40 years of age. This set of simulations was performed to analyze the wall strength under conditions of ground confinement, which was appropriate for representing the

mechanical circumstances of the wall. The purpose of this simulation was to verify that the concrete was properly designed for the conditions in which it was located. The analysis results yielded a compressive strength that was significantly higher than the maximum pressure loaded onto the specimen owing to the self-weight of the wall; thus, the wall is predicted to remain stable under these conditions for a service life of 40 years.

The fourth step, encompasses the effect of confinement, representing the ground pressure, showed an extremely positive impact on wall stability, preventing failure due to material degradation caused by aggressive environmental conditions.

In comparing our approach to quantifying the porosity volume obtained from microsimulation on the cement paste scale when subjected to the leaching effect to experimental results found in the literature, we found a perfect fit between methods. Therefore, the suggested method has proven to be an accurate tool for predicting the behavior of concrete subjected to aggressive environmental conditions.

Funding

This study was funded by the Ministry of Science, Technology, and Space, Government of Israel, (COST Action TU1404), and Planning and Budgeting Committee (PBC). *Ethical standards:* The authors declare that they have complied with all relevant ethical standards. *Consent to participate:* All participants consent to participate in the present study *Consent for publication.*

CRediT authorship contribution statement

G. Lifshitz Sherzer: Conceptualization, Methodology, Validation, Formal analysis, Investigation, Resources, Data curation, Writing – original draft, Writing – review & editing, Visualization. **G. Ye:** Conceptualization, Methodology, Resources, Writing – review & editing, Supervision, Project administration. **E. Schlangen:** Conceptualization, Methodology, Resources, Writing – review & editing, Supervision, Project administration. **K. Kovler:** Conceptualization, Methodology, Resources, Writing – review & editing, Supervision, Project administration.

Declaration of Competing Interest

The authors declare that they have no known competing financial interests or personal relationships that could have appeared to influence the work reported in this paper.

Acknowledgments

This research was supported by the Ministry of Science, Technology, and Space, Government of Israel; the European Concerted Research Action TU 1404 titled “Towards the Next Generation of Standards for Service Life of Cement-Based Materials and Structures”; and Planning & Budgeting Committee (Council for higher education). The authors are thankful to Prof. Erez Gal for his valuable advice and support throughout the work.

References

- [1] S. Frydman, J. Charrach, I. Goretsky, A geotechnical study of evaporitic, lacustrine sediments in the saline environment of the Dead Sea area, *Eng. Geol.* 181 (2014) 309–322, <https://doi.org/10.1016/j.enggeo.2014.08.028>.
- [2] W. Wittke, M. Wittke, A. Zakin, Dike rehabilitation by construction of an 18-km long slurry trench wall at the Dead Sea, Israel, in: *Twenty-Sixth Int. Congr. Large Dams*, 4–6 July 2018, Vienna, Austria (1st Ed.). CRC Press, International Commission on Large, 2018. <https://doi.org/10.1201/9780429465086>.
- [3] C. Heim, N.R. Nowaczyk, J.F.W. Negendank, S.A.G. Leroy, Z. Ben-Avraham, *Near East desertification: evidence from the Dead Sea*, *Naturwissenschaften* 84 (9) (1997) 398–401.
- [4] F. Kato, Y. Suwa, K. Watanabe, S. Hatogai, Mechanisms of coastal dike failure induced by the Great East Japan Earthquake Tsunami, *Proc. Coast. Eng. Conf.* 1 (2012) 1–9. https://www.engineeringvillage.com/share/document.url?mid=cpx_M26977100141eb1338abM69f92061377553&database=cpx.
- [5] K. Kovler, V. Chernov, *Failure, Distress and Repair of Concrete Structures*, Woodhead Publishing Limited, Cambridge, 2009.
- [6] O. Matsuo, Damage to river dikes, *Soils Found.* 36 (1996) 235–240, https://doi.org/10.3208/sandf.36.Special_235.
- [7] E. Guillon, M. Moranville, S. Kamali, Characterization of the mechanical damage of a chemically degraded cement paste, *Mater. Struct. Constr.* 39 (2006) 401–409, <https://doi.org/10.1617/s11527-005-9011-x>.
- [8] C. Carde, *Caractérisation et modélisation de l’altération des propriétés mécaniques due à la lixiviation des matériaux cimentaires*, INSA, Toulouse, 1996 <http://www.theses.fr/1996ISAT0010>.
- [9] M. Mainguy, F.-J. Ulm, F.H. Heukamp, Similarity properties of demineralization and degradation of cracked porous materials, *Int. J. Solids Struct.* 38 (2001) 7079–7100, [https://doi.org/10.1016/S0020-7683\(00\)00417-0](https://doi.org/10.1016/S0020-7683(00)00417-0).
- [10] F. Bernard, S. Kamali-Bernard, W. Prince, 3D multi-scale modelling of mechanical behaviour of sound and leached mortar, *Cem. Concr. Res.* 38 (4) (2008) 449–458.
- [11] E. Koenders, *Simulation of Volume Changes in Hardening Cement-Based Materials*, Doctoral Thesis. TU Delft, The Netherlands, 1997.
- [12] K. Van Breugel, *Simulation of Hydration and Formation of Structure in Hardening Cement-Based Materials*, Doctoral Thesis. TU Delft, The Netherlands, 1993.
- [13] G. Ye, *Experimental Study and Numerical Simulation of the Development of the Microstructure and Permeability of Cementitious Materials*, Doctoral Thesis. TU Delft, The Netherlands, 2003.
- [14] G. Ye, K. Van Breugel, A.L.A. Fraaij, Three-dimensional microstructure analysis of numerically simulated cementitious materials, *Cem. Concr. Res.* 33 (2003) 215–222, [https://doi.org/10.1016/S0008-8846\(02\)00889-X](https://doi.org/10.1016/S0008-8846(02)00889-X).
- [15] P. Rosin, E. Rammner, The laws governing the fineness of powdered coal, *Inst. Fuel*, 7 29–36. *Eval. Folk Ward Graph. Meas. J. Sediment. Res.* 48. (1933) 863–878.
- [16] Z. Qian, E. Schlangen, G. Ye, K. Van Breugel, Prediction of mechanical properties of cement paste at microscale, *Mater. Constr.* 60 (2010) 7–18, <https://doi.org/10.3989/mc.2010.55209>.
- [17] Z. Qian, *Multiscale modeling of fracture processes in cementitious materials*, Doctoral Thesis. TU Delft, The Netherlands, 2012. <https://www.narcis.nl/publication/RecordID/oa:tudelft.nl:uuid%3A734b276c-283a-4f7a-8db2-a184453e8dac>.
- [18] Z. Qian, E. Schlangen, G. Ye, K. Van Breugel, Multiscale lattice fracture model for cement-based materials, in: *ICCM 2012 4th Int. Conf. Comput. Methods, Gold Coast, Aust.* 25–28 Novemb. 2012, 2012.
- [19] E. Schlangen, J.G.M. van Mier, Experimental and numerical analysis of micromechanisms of fracture of cement-based composites, *Cem. Concr. Compos.* 14 (1992) 105–118, [https://doi.org/10.1016/0958-9465\(92\)90004-F](https://doi.org/10.1016/0958-9465(92)90004-F).
- [20] Z. Qian, E.J. Garboczi, G. Ye, E. Schlangen, Anm: a geometrical model for the composite structure of mortar and concrete using real-shape particles, *Mater. Struct. Constr.* 49 (2016) 149–158, <https://doi.org/10.1617/s11527-014-0482-5>.
- [21] G. Lifshitz Sherzer, E. Schlangen, G. Ye, A.E. Gal, Evaluating compressive mechanical LDPM parameters based on an upscaled multiscale approach, *Constr. Build. Mater.* 251 (2020) 1–18. <https://doi.org/10.1016/j.conbuildmat.2020.118912>.
- [22] F.-J. Ulm, O. Coussy, K. Li, C. Larive, Thermo-chemo-mechanics of ASR expansion in concrete structures, *J. Eng. Mech.* 126 (2000) 233–242, [https://doi.org/10.1061/\(ASCE\)0733-9399\(2000\)126:3\(233\)](https://doi.org/10.1061/(ASCE)0733-9399(2000)126:3(233)).
- [23] Z.P. Bazant, F.C. Bishop, T.-P. Chang, Confined compression tests of cement paste and concrete up to 300 ksi, *J. Am. Concr. Inst.* 83 (1986) 553–560. https://www.engineeringvillage.com/share/document.url?mid=cpx_2001388&database=cpx.
- [24] M. Nikoo, F. Torabian Moghadam, E. Sadowski, Prediction of concrete compressive strength by evolutionary artificial neural networks, *Adv. Mater. Sci. Eng.* 2015 (2015) 1–8, <https://doi.org/10.1155/2015/849126>.
- [25] U. Mallast, C. Siebert, B. Wagner, M. Sauter, R. Gloaguen, S. Geyer, R. Merz, Localisation and temporal variability of groundwater discharge into the Dead Sea using thermal satellite data, *Environ. Earth Sci.* 69 (2013) 587–603, <https://doi.org/10.1007/s12665-013-2371-6>.
- [26] M. Rais, *Manual for Civil Engineers*, in: Masada Publ., Isr., 1980.
- [27] G. Sherzer, P. Gao, E. Schlangen, G. Ye, E. Gal, Upscaling cement paste microstructure to obtain the fracture, shear, and elastic concrete mechanical LDPM parameters, *Materials (Basel)*. 10 (2017) 242, <https://doi.org/10.3390/ma10030242>.
- [28] H. Manzano, J.S. Dolado, A. Ayuela, Elastic properties of the main species present in Portland cement pastes, *Acta materialia* 57 (5) (2009) 1666–1674, <https://doi.org/10.1016/j.actamat.2008.12.007>.
- [29] E.J. Garboczi, D.P. Bentz, Computer simulation and percolation theory applied to concrete, *Annu. Rev. Comput. Phys.* VII. 85 (1999), https://doi.org/10.1142/9789812813329_0004.
- [30] F.H. Heukamp, *Chemomechanics of calcium leaching of cement-based materials at different scales: the role of CH-dissolution and C-S-H degradation on strength and durability performance of materials and structures*, Massachusetts Institute of Technology (2003). <https://dspace.mit.edu/handle/1721.1/29282>.